HHS Public Access

Author manuscript

Small. Author manuscript; available in PMC 2026 January 01.

Published in final edited form as:

Small. 2025 January ; 21(1): e2406389. doi:10.1002/smll.202406389.

Optomagnetic Micromirror Arrays for Mapping Large Area Stiffness Distributions of Biomimetic Materials

Hsin Lan[1], **Marvin Tan Xin Haw**[2], **Minh-Tam Tran Le**[2], **Hao-Yu Chien**[5], **Ruoda Zheng**[1], **Amy C. Rowat**[2,4], **Michael A. Teitell**[2,3], **Pei-Yu Chiou**[1,2]

[1]Department of Mechanical and Aerospace Engineering, University of California Los Angeles, Los Angeles, California, USA.

[2]Department of Bioengineering, University of California Los Angeles, Los Angeles, California, USA.

[3]Department of Pathology and Laboratory Medicine, David Geffen School of Medicine, University of California Los Angeles, Los Angeles, California, USA.

[4]Department of Integrative Biology & Physiology, University of California Los Angeles, Los Angeles, California, USA.

[5]Department of Electrical and Computer Enigeering, University of California Los Angeles, Los Angeles, California, USA.

Abstract

We demonstrated a new device termed "Optomagnetic Micromirror Arrays" (OMA) capable of mapping the stiffness distribution of biomimetic materials across a 5.1 mm × 7.2 mm field of view with cellular resolution. The OMA device comprises an array of 50,000 magnetic micromirrors with optical grating structures embedded beneath an elastic PDMS film, with biomimetic materials affixed on top. Illumination of a broadband white light beam onto these micromirrors results in reflection of microscale rainbow light rays on each micromirror. When a magnetic field is applied, it causes each micromirror to tilt differently depending on the local stiffness of the biomimetic materials. Through imaging these micromirrors with low N.A. optics, a specific narrow band of reflection light rays from each micromirror is captured. Changing a micromirror's tilt angle also alters the color spectrum it reflects back to the imaging system and the color of the micromirror image it represents. As a result, OMA can infer the local stiffness of the biomimetic materials through the color change detected on each micromirror. OMA offers the potential for high-throughput stiffness mapping at the tissue-level while maintaining the spatial resolution at the cellular level.

Graphical Abstract

We developed an Optomagnetic Micromirror Array (OMA) device for stiffness mapping of biomimetic materials. The array of 50,000 micromirrors diffracts light into microscale rainbows, tilting according to the local stiffness of materials when a uniform magnetic field is applied. By capturing reflected light spectra, OMA detects stiffness variations across a 5.1 mm × 7.2 mm field with single-cell resolution, enabling high-throughput tissue-level mapping.

INTRODUCTION

In recent years, there have been significant and growing interests in tissue and cellular mechanics as potential indicators of health or disease[1]. Properties of interest are those that provide information on the mechanical responses of cells to external stimuli, such as mechanical forces applied in the extracellular environment and have emerged as key biomarkers for evaluating cellular behaviors and functions. For example, cells with a well-organized cytoskeleton structure tend to be stiffer and more resistant to deformation than cells with a disorganized cytoskeleton[2]. The reorganization of cytoskeletal elements can be triggered by pathological process[3] and the correlation between cell stiffness and the presence of cell pathology has been extensively studied[1,4]. Non-physiologic variations in cell stiffness have been noted in multiple diseases, such as cancer[5], cardiovascular disease[6], and neurological disorders[7]. Among these, has captured significant investigative interest. It has been widely reported that most cancerous cells exhibit lower stiffness than their benign counterpart cells[1,8], which could be a feature of the compliance needed to facilitate movement during metastatic processes. Supporting this idea, recent studies have established a strong link between the cellular phenotype, particularly cellular stiffness, and the metastatic potential of cancer cells[9,10]. Highly metastatic cells typically express fewer surface adhesion receptors and exhibit increased protease activity, which helps them detach from their surroundings[10]. Multiple studies have shown that cancer cells with lower stiffness are more likely to metastasize than those with higher stiffness[11,12].

Recent technological advancements have facilitated measurement of cellular stiffness in vitro, with technologies that include AFM[8,9,12], micropipette aspiration[13,14], optical tweezers[15-18], and magnetic twisting cytometry[10,19-22]. These approaches enable researchers to gain a better understanding of the relationship between cellular mechanics and cellular behavior. While current approaches can provide high spatial resolution for probing cellular stiffness, they are constrained by small cell population assessments and low throughput. Although mechanical properties of isolated single cells can provide informative clues for detecting changes in cellular states or diseases, most disease developments involve collective cell migration and tissue reorganization. For instance, the presence of leader cells and follower cells is observed in collectively migrating and invading cancer cells[23,24]. A study from Swaminathan *et al.* established a correlation between cellular stiffness and invasiveness in cancer cells through the measurement with magnetic tweezers[10]. A study from Lekka *et al.* showed that the Young's modulus of different cancer cells increases with cell populations and densities[8]. On an even larger spatial scale, tissue stiffness can be a revealing indicator of disease states. Generally, tissues are a collection of heterogeneous cell types that form three dimensional layers interwoven with extracellular matrix (ECM) elements. The ECM has multifaceted roles including, for example, supporting the repair of wounds or can perversely advance tumor progression[25]. Studies in breast cancer have shown significant changes in tissue properties, with tissue stiffness potentially increasing up to tenfold compared to normal breast tissue.[26,27]. These studies have also revealed that the regions of increased tissue stiffness often located at the margins of invasive tumors. Since cancer cells are usually softer than their non-malignant counterparts, these findings

underscore the critical influence of the ECM and potentially heterogeneous non-malignant cell types on tissue stiffness and tumor behavior[8].

Available techniques for measuring tissue stiffness can be broadly categorized into those that assess tissue samples as bulk materials, such as tensile testing[28,29] and compression testing[29], and those that probe local stiffness, such as AFM[30] and micropipette techniques[31]. Bulk material property measurements provide an average value and do not represent the variable characteristics of heterogenous samples. On the other hand, while tools like AFM offer detailed nanoscale measurements of heterogenous samples, they are low throughput and fall short in measuring larger-scale stiffness variations driven by changes in cellular and ECM structures. Therefore, a new type of platform capable of measuring across length scales from cellular to supracellular or mesoscopic is needed to reveal how changes and interactions in cellular and extracellular structures affect dynamic stiffness[32].

Here, we introduces the first high-throughput platform called Optomagnetic Micromirror Arrays (OMA), which enables the mapping of stiffness distributions in biomimetic materials across a 5.1 mm × 7.2 mm area, with cellular-level spatial resolution. OMA comprises more than 50,000 magnetic micromirrors with submicron optical grating structures affixed to a flexible PDMS thin film (Figure 1A). The operation principle of OMA is by applying an uniform magnetic field (B) at a specific angle to the platform. The magnetic micromirrors are tilted by the magnetic field due to the shape anisotropic magnetization effect. The tilting angle of each micromirror is determined by the local stiffness of the PDMS substrate and the biomimetic material above it. Therefore, with known PDMS stiffness information as a reference, the local stiffness of biomimetic material above each micromirror can be directly extracted from its tilting angle. To detect the tilting angles of all 50,000 magnetic micromirrors, we apply a broadband white light source illumination on the OMA platform. The optical grating structure on each micromirror reflects the white light and introduces different reflection angles on different wavelengths of light, equivalent to generating a microscale rainbow on each micromirror. By properly choose a low N.A. optics for imaging these micromirrors, only a narrow band of color spectrum reflected by each micromirror can fall in the collection angle of this low N.A. optics (dotted lines in the inset of Figure 1A). The image of each micromirror projected onto the sensor of a color camera will only consist these collected spectra, giving a representative color indicating the tilting angle of that micromirror (lower left, Figure 1A). If a micromirror is tilted to a different angle, it changes the collected spectra and its representative color. Therefore, by monitoring the color change of a micromirror's image, its dynamic tilting angle can be measured in real-time at a video frame rate.

As the field of view (FOV) is considerably large (5.1 mm × 7.2 mm), the micromirrors located at the opposite ends of the device will experience different incident angles under the same illumination (Figure 1B, left), resulting in varying detected colors even if all the micromirrors have the same tilting angle. Consequently, the detected colors across the entire FOV will exhibit a color gradient from one side to the other. To quantify the correlation between color, tilting angles, and locations, we calibrate the color-to-tilt relationship. (see Supplementary Materials Figure S4). After uniform magnetic actuation, all the micromirrors will tilt to a certain angle, causing the entire spectrum to exhibit a color gradient with a blue

shift (Figure 1B, right). Figure 1C shows the OMA device before magnetic actuation, while Figure 1D displays the device after the magnetic field tilts. It is evident from the image that the micromirrors undergo a blue shift due to the mechanical torque induced by the effect of magnetic shape anisotropy.

Figure 2 illustrates various scenarios involving biomimetic materials with different stiffness levels and shapes covering micromirrors, showing the resulting relative collection spectrum changes compared to the case where no material covers the micromirrors. On the current OMA platform, tilting angles of 50,000 micromirrors can be concurrently measured to extract the stiffness distribution of a biomimetic material over an area of 35 mm^2.

Results

Imaging System and Grating Design

The OMA platform quantifies the stiffness of biomimetic materials through the analysis of the color spectra reflected by an array of micromirrors with surfaces patterned with optical grating structures. These micromirrors are subjected to broadband white light illumination. The micromirror images are captured using a Canon color camera equipped with an MP-E 65mm f/8 optical lens (see Materials and Methods for details). The technical details of the optical design used here have also been reported in our previous work.[33]. When the magnetic field tilts the micromirrors, the color spectra detected from each micromirror change. This change encodes the information about the local stiffness of the biomimetic materials attached to the non-grating surface of the micromirror on top of the PDMS platform layer.

Since the broadband white light is illuminated at an angle, the correlation between incidence and diffraction can be quantified by the grating equation:

$$\sin\theta_m = \sin\theta + m\frac{\lambda}{\Lambda}$$

where m denotes as the m^{th} order of diffraction (with negative values indicating orders on the same side as the incident light in relation to the normal) and θ represents the angle between the direction of light and normal, λ is the wavelength of diffracted light, and Λ is the grating period. On the OMA platform, the optical grating period is 1.2 μm and the incident angle of while light is 66°. We choose the 2^{nd} order diffraction band for detection and position the 532nm wavelength of light at the midpoint of this 2^{nd} order band.

Magnetic Actuation and Design

A magnetic field is applied to the OMA platform to tilt the micromirrors based on the magnetic shape anisotropy effect, where the magnetization strength inside a magnetic material depends on its shape or geometry. This effect occurs when the shape of a magnetic material is not symmetric, causing the magnetization to be preferentially oriented in one direction over another. OMA micromirrors are made of the magnetic material cobalt (Co) and have a circular disk shape. Their easy magnetization axes align with the surface of the device. To tilt the micromirrors, we employ two N52 grade permanent magnets (K&J

Magnetics Inc.) separated by a distance of 2.25 inches (Figure S1A). This configuration establishes a uniform magnetic field of 211 mT spanning the entire OMA platform (Figure S1B-D), providing uniform magnetic forces on all micromirrors. When the magnetic field is angled relative to the easy axes of the micromirrors, it generates the shape-anisotropic magnetization effect and induces mechanical torques on micromirrors embedded in a PDMS substrate with a Young's modulus of 42 kPa (see Materials and Methods, Figure S2).

Mechanical Decoupling

Since the micromirror arrays are embedded in a continuous PDMS film, the potential coupling effect between neighboring micromirrors needs to be considered. To understand the degree of coupling, we used the finite element method (FEM) in COMSOL Multiphysics for simulation. We studied the case where a Co micromirror is surrounded by non-magnetic silicon (Si) micromirrors with a 26 μm pitch (Figure 3A). Figures 3B and 3C depict the volumetric strain and displacement around the central Co micromirror when a magnetic field is applied. The results show that when the central Co micromirror is tilted by 5.24°, adjacent micromirrors tilt by only 0.03°, which is less than 1% (Figure 3D). Therefore, we conclude that the mechanical coupling effect between neighboring micromirrors on the OMA platform with the current pitch seperation can be neglected. This provides a major advantage and greatly simplifies the stiffness measurement process since the local stiffness can be directly read from the color of the dot-like image of a micromirror without using complex computational methods.

Sample Thickness Effect

The shapes of living cells or tissues are not uniform, and their thicknesses can vary at different areas on the OMA device. For instance, individual cells often exhibit a bell-shaped structure when adhered to a flat surface. This results in marginal areas with thicknesses as low as 1 μm or less[34], whereas the region at the nucleus can extend to around 8 μm or more in height[35]. Similar variations are also observed in collective cell sheets[36,37], where the edges are often an order of magnitude thinner than the majority. The thickness variation can be even more complex for biological tissues, where ECM and heterogenous cell types are presence[30,38]. Such thickness variability can introduce errors in measuring tissue stiffness using our OMA method. Therefore, we simulated the effect of tissue thickness on the micromirrors' tilting angle under magnetic rotation. In Figure 3E, the COMSOL model depicts 25 Co micromirrors sandwiched between a tissue layer of 5 kPa stiffness that varies in thickness from 1 to 25 μm, and a 42 kPa PDMS substrate with a thickness of 30 μm. As illustrated in Figure 3F, the tilting angle gradually reduces with increasing tissue thickness, plateauing when the thickness exceeds 10 μm. We investigated this effect with tissues of different stiffness and reach the same conclusion (25 kPa and 50 kPa in Figure 3F). This outcome suggests that our platform is suited for measuring tissue samples of thicknesses larger than 10 μm; for thickness less than 10 μm, the thickness factor will need to be considered.

Characterization of Young's Modulus of Biomimetic PDMS thin films

To assess the capability of the OMA platform's capability for measuring cell-like stiffness using PDMS as a surrogate material, we conducted both experimental evaluations and

simulation modeling to establish the relationship between the micromirror tilting angles and the Young's modulus of PDMS in the range of 0-200 kPa.

For experimental evaluation, we attach PDMS samples of different stiffness levels, simulating the spectrum of soft biological cells and tissues, to different regions on the OMA device. The stiffness of the PDMS samples was adjusted by controlling the mixing ratio of precursors (Table 1). By tilting the magnetic field, we actuate the micromirror arrays and measure their changes in tilting angles in each of these regions. To counter the optical scattering noise arising from the PDMS-air interfaces, we introduced a black PDMS film formulated with carbon nanotubes (CNTs) into the PDMS mixture (Figure S7) to absorb the scattered light. Subsequently, we spin-coated the PDMS for measurement onto a small piece of the CNT-PDMS sheet, forming a composite sample. This composite is flipped and placed onto the micromirror platform before curing the PDMS, ensuring minimal disruption to the micromirrors. This procedure was repeated for different regions across the OMA device for all PDMS samples with varying stiffness levels. The PDMS thin films were allowed to naturally cure at room temperature for 24 hours.

Figure 4A illustrates a map depicting the net tilting angle change (Δt) across the entire 5.1 mm × 7.2 mm FOV on an OMA device during the stiffness measurement procedure. Each data point on the map corresponds to a single micromirror. The white data points represent defective micromirrors from microfabrication. This map was created by subtracting the tilting angles of each micromirror after magnetic actuation from those before actuation. The results outline distinct regions (a-i) corresponding to PDMS samples of varying stiffness, each demonstrating different degrees of tilting angle change. We computed the average tilting angle change for each area and used it for Young's modulus calculation. Notably, the open area (region a, without any material attached) shows an average tilting angle of 3.66 degrees, which will be used as a baseline tilting angle in the simulation modeling section.

We calibrated the Young's modulus of each PDMS sample using nanoindentation (Pavone, Optics11 Life). To ensure consistency in material properties between the PDMS samples on the OMA platform and those used for nanoindentation, during the preparation of the CNT-PDMS composite samples for OMA measurements, we also prepared an additional sample for each PDMS variation on a glass substrate with the same spin coating parameters for nanoindentation measurements (Figure S7E). Subsequently, we incorporated the Young's modulus data from the nanoindentation measurements into our results obtained on the OMA platform to establish the relationship between tilting angle change and the Young's modulus of the PDMS samples (Figure 4B).

Of note is that the thickness (>30 μm) of the PDMS films used in the testing is much larger than the effective deformation range of a tilting micromirror (10 μm, Figure 3F). If the PDMS thin film or the tissues to be measured have a thickness thinner than this effective range, a correction factor will need to be added to account for the thickness effect. Furthermore, because the effective range of mechanical coupling is considerably shorter (Figure 3A-D) than the spacing between micromirrors (26 μm), we can disregard this coupling factor. This means that the change in tilting angle at each micromirror directly indicates the local stiffness information. This substantially simplifies data interpretation

on the OMA platform, eliminating the need to decode the complex coupling relationships between neighboring tracer particles as seen in previous studies[19,22].

In the simulation, we applied the finite element method (FEM) using COMSOL Multiphysics to model a device with a 5×5 Co micromirror array (Figure 5A) sandwiched between a layer of biomimetic tissue with varying Young's modulus and a PDMS substrate. We measured the micromirrors' magnetization hysteresis (MH) loop using a magnetometer (MPMS3, Quantum Design Applications Inc.) and the PDMS substrate's Young's modulus via nanoindentation (Pavone, Optics11 Life). These parameters were subsequently input into the model to determine the effective magnetic torque that produces a tilting angle of 3.66 degrees—matching the tilting angle of region "a" in Figure 4A. This establishes a common baseline for comparison between the simulation and experimental data. We navigated a range of Young's modulus values between 0-200 kPa with 2.5 kPa increments to quantify the relationship between the PDMS Young's modulus and tilting angles. We applied a curve fitting model (PyEarth) to process the data, revealing an exponential-like curve (Figure 5B).

In addition, we compared the experimental data points with the simulated curve, as depicted in Figure 5C. There is a close agreement between the simulation curve and the experimentally obtained averaged Young's modulus at different regions, showing an R^2 score of 0.95 (Figure 5D). This finding indicates that the curve derived from simulation modeling can serve as a reliable calibration curve for quantifying the stiffness of biomimetic materials within the range of 0-200 kPa.

PDMS Young's Modulus Measurement and Validation

With the validated calibration curve revealing the relationship between materials' Young's modulus and the tilting angle of micromirrors on the OMA platform (Figure 5B), we can convert the tilting angle map in Figure 4A into the stiffness distribution map (Figure 6A). It should be noted that the stiffness map shows clear boundaries between different PDMS areas (inset, Figure 6A). This indicates that the OMA device can achieve a spatial resolution of 26 μm, the pitch of the micromirrors. This level of resolution corresponds to single adherent mammalian cell when adhering and extending on a substrate[9][12][18][20][21][39].

Figure 6B compares the results measured by the OMA platform and those measured by nanoindentation. Clearly, although the averaged Young's moduli measured by the OMA platform at different regions closely match the nanoindentation data, the data from the OMA platform shows a larger variation (~30%) between micromirrors in the same region. This variation can arise from several causes, which will be discussed in the Discussion section and will need to be addressed in future studies.

Discussion

The demonstrated OMA platform can potentially offer several advantages over prior methods mapping tissue stiffness distributions. First, OMA provides concurrent and large-scale assessments, promising the analysis of tens of thousands of cells at once due to the large device area it covers. Second, OMA features a self-referential measurement capability. The absolute tilt of each micromirror is represented by its specific color code, eliminating

the need for using adjacent structures or particles for position or angle calibration, which is a typical prerequisite in prevailing traction force microscopy methods [19-22,40]. As a result, the local stiffness near a micromirror can be determined based on the variation of its tilting angle before and after magnetic actuation. This approach is valid even in scenarios where neighboring micromirrors are connected by a continuous film. The stiffness reading on each micromirror is independent of the others.

Although the current work focuses on demonstrating the proof-of-concept stiffness measurement for passive biomimetic materials, it is important to consider that cells are active materials and can exert forces to tilt the micromirrors even without an applied magnetic field. For accurate stiffness measurement, it is essential to disentangle the cell-induced tilting angles from the micromirrors. To achieve this, we can detect the tilting angles induced by cells before and after a magnetic field is applied. The difference between these two tilting angles can be used to extract the stiffness information. In fact, this approach has already been used in Figure 4A to obtain the micromirror tilting angle difference before and after applying a magnetic field, thus removing the initial tilting angles induced by bonding the PDMS thin films on the OMA platform.

The current OMA platform can be further improved in two aspects for future stiffness measurements in real biological tissue samples. Two technical challenges need to be overcome. First, based on the data shown in Figure 6B, although the averaged Young's moduli measured at different PDMS regions on the OMA platform match well with the calibration data from a nanoindenter, the data from the OMA platform shows a large variation (~30%) between micromirrors located in the same PDMS sample region. The cause of such variation is most likely attributed to light scattering from the edges of micromirrors. Light scattered by the edges of micromirrors depends on their tilting angle. This angle-dependent scattering mechanism is different from the optical grating principle used by OMA. This effect is manifested by the non-uniform color distribution on each of the dot-like light spots that represent the image of a micromirror. From the three zoomed images shown in the upper right region of Figure 1B, the color spectra from the pixels located at the upper or bottom edges of these dots are different from other pixels. In our current algorithm (Gaussian fitting) to extract the representative RGB color from each dot-like image of a micromirror, these non-uniform color distributions are smoothed out and become noise in the Gaussian-fitted RGB values. Therefore, to mitigate this issue in the future, the edge scattering effect needs to be suppressed to minimize the variation between micromirrors.

Second, the current OMA platform needs improved device stability when operating in physiological buffers. In the current device, the composite Ti/Co/Al layer on a micromirror is sealed by a thin SiO_2 layer deposited via the PECVD method. This SiO_2 layer is susceptible to developing pinholes, which compromises its ability to effectively isolate the buffer medium. Consequently, this composite metal layer oxidizes when culturing cells on the device, leading to the degradation of both the magnetic and optical properties of the micromirror. One potential solution to address this oxidation issue is to substitute the current SiO_2 layer with pinhole-free aluminum oxide (Al_2O_3) deposited through atomic layer deposition (ALD).

Conclusion

The mechanical stiffness of tissue samples has emerged as a valuable indicator for differentiating disease or cellular states. However, existing techniques for measuring tissue stiffness are limited in their ability to assess only a small number of cells, making concurrent evaluation of large area samples difficult. This limitation hampers the investigation of collective cell behaviors and dynamic tissue structure changes during disease progression. The demonstrated Optomagnetic Micromirror Arrays (OMA) platform has the potential to address these limitations by employing over 50,000 magnetic micromirrors with optical grating nanostructures embedded in an elastic PDMS substrate. With a FOV of 5.1 mm × 7.2 mm, the OMA platform is strongly positioned to enable tissue-level measurements. Each individual micromirror can be magnetically actuated to measure the local stiffness of biomimetic material with single-cell spatial resolution. The calibrated OMA platform is capable of quantifying the elastic modulus of biomimetic materials within the range of 0-200 kPa, which encompasses the stiffness range commonly observed in biological tissues and cells.

Supplementary Material

Refer to Web version on PubMed Central for supplementary material.

Acknowledgement

This research is supported by the National Institutes of Health (NIH) R01GM127985, and NSF CMMI 2029454, NSF DBI 2345571 and a NSF BRITE Fellow Award to ACR (CMMI-2135747).

Reference

[1]. Suresh S, Acta Biomater. 2007, 3, 413. [PubMed: 17540628]

[2]. Luo Q, Kuang D, Zhang B, Song G, Biochim. Biophys. Acta BBA - Gen. Subj 2016, 1860, 1953.

[3]. Kumar Y, Valdivia RH, Commun. Integr. Biol 2008, 1, 175. [PubMed: 19704885]

[4]. Dulińska I, Targosz M, Strojny W, Lekka M, Czuba P, Balwierz W, Szymoński M, J. Biochem. Biophys. Methods 2006, 66, 1. [PubMed: 16443279]

[5]. Suresh S, Nat. Nanotechnol 2007, 2, 748. [PubMed: 18654425]

[6]. Ferrari S, Pesce M, Int. J. Mol. Sci 2021, 22, 3404. [PubMed: 33810253]

[7]. Wang L, Xia J, Li J, Hagemann TL, Jones JR, Fraenkel E, Weitz DA, Zhang S-C, Messing A, Feany MB, Nat. Commun 2018, 9, 1899. [PubMed: 29765022]

[8]. Lekka M, BioNanoScience 2016, 6, 65. [PubMed: 27014560]

[9]. Xu W, Mezencev R, Kim B, Wang L, McDonald J, Sulchek T, PLOS ONE 2012, 7, e46609. [PubMed: 23056368]

[10]. Swaminathan V, Mythreye K, O'Brien ET, Berchuck A, Blobe GC, Superfine R, Cancer Res. 2011, 71, 5075. [PubMed: 21642375]

[11]. Watanabe T, Kuramochi H, Takahashi A, Imai K, Katsuta N, Nakayama T, Fujiki H, Suganuma M, J. Cancer Res. Clin. Oncol 2012, 138, 859. [PubMed: 22297840]

[12]. Liu H, Tan Q, Geddie WR, Jewett MAS, Phillips N, Ke D, Simmons CA, Sun Y, Cell Biochem. Biophys 2014, 68, 241. [PubMed: 23793959]

[13]. Rowat AC, Lammerding J, Ipsen JH, Biophys. J 2006, 91, 4649. [PubMed: 16997877]

[14]. Shojaei-Baghini E, Zheng Y, Jewett MAS, Geddie WB, Sun Y, Appl. Phys. Lett 2013, 102, 123704.

[15]. Guck J, Schinkinger S, Lincoln B, Wottawah F, Ebert S, Romeyke M, Lenz D, Erickson HM, Ananthakrishnan R, Mitchell D, Käs J, Ulvick S, Bilby C, Biophys. J 2005, 88, 3689. [PubMed: 15722433]

[16]. Zhang H, Liu K-K, J. R. Soc. Interface 2008, 5, 671. [PubMed: 18381254]

[17]. Neuman KC, Block SM, Rev. Sci. Instrum 2004, 75, 2787. [PubMed: 16878180]

[18]. Suresh S, Spatz J, Mills JP, Micoulet A, Dao M, Lim CT, Beil M, Seufferlein T, Acta Biomater. 2005, 1, 15. [PubMed: 16701777]

[19]. De Vlaminck I, Dekker C, Annu. Rev. Biophys 2012, 41, 453. [PubMed: 22443989]

[20]. Chen L, Maybeck V, Offenhäusser A, Krause H-J, Rev. Sci. Instrum 2016, 87, 064301. [PubMed: 27370475]

[21]. Mohagheghian E, Luo J, Yavitt FM, Wei F, Bhala P, Amar K, Rashid F, Wang Y, Liu X, Ji C, Chen J, Arnold DP, Liu Z, Anseth KS, Wang N, Sci. Robot 2023, 8, eadc9800. [PubMed: 36696474]

[22]. Bausch AR, Möller W, Sackmann E, Biophys. J 1999, 76, 573. [PubMed: 9876170]

[23]. Friedl P, Locker J, Sahai E, Segall JE, Nat. Cell Biol 2012, 14, 777. [PubMed: 22854810]

[24]. Vilchez Mercedes SA, Bocci F, Levine H, Onuchic JN, Jolly MK, Wong PK, Nat. Rev. Cancer 2021, 21, 592. [PubMed: 34239104]

[25]. Handorf AM, Zhou Y, Halanski MA, Li W-J, Organogenesis 2015, 11, 1. [PubMed: 25915734]

[26]. Butcher DT, Alliston T, Weaver VM, Nat. Rev. Cancer 2009, 9, 108. [PubMed: 19165226]

[27]. Kass L, Erler JT, Dembo M, Weaver VM, Int. J. Biochem. Cell Biol 2007, 39, 1987. [PubMed: 17719831]

[28]. Cooney GM, Moerman KM, Takaza M, Winter DC, Simms CK, J. Mech. Behav. Biomed. Mater 2015, 41, 68. [PubMed: 25460404]

[29]. Griffin M, Premakumar Y, Seifalian A, Butler PE, Szarko M, J. Vis. Exp. JoVE 2016, 54872. [PubMed: 28060331]

[30]. Jorba I, Uriarte JJ, Campillo N, Farré R, Navajas D, J. Cell. Physiol 2017, 232, 19. [PubMed: 27163411]

[31]. Ozawa H, Matsumoto T, Ohashi T, Sato M, Kokubun S, J. Neurosurg. Spine 2001, 95, 221.

[32]. Xavier da Silveira dos Santos A, Liberali P, Febs J. 2019, 286, 1495. [PubMed: 30390414]

[33]. Marvin Tan XH, Wang Y, Zhu X, Mendes FN, Chung P-S, Chow YT, Man T, Lan H, Lin Y-J, Zhang X, Zhang X, Nguyen T, Ardehali R, Teitell MA, Deb A, Chiou P-Y, Biosens. Bioelectron 2024, 258, 116318. [PubMed: 38701538]

[34]. Calzado-Martín A, Encinar M, Tamayo J, Calleja M, San Paulo A, ACS Nano 2016, 10, 3365. [PubMed: 26901115]

[35]. Bastatas L, Martinez-Marin D, Matthews J, Hashem J, Lee YJ, Sennoune S, Filleur S, Martinez-Zaguilan R, Park S, Biochim. Biophys. Acta BBA - Gen. Subj 2012, 1820, 1111.

[36]. Poole K, Meder D, Simons K, Müller D, FEBS Lett. 2004, 565, 53. [PubMed: 15135052]

[37]. Hoh JH, Schoenenberger C-A, J. Cell Sci 1994, 107, 1105. [PubMed: 7929621]

[38]. Mao Y, Sun Q, Wang X, Ouyang Q, Han L, Jiang L, Han D, Appl. Phys. Lett 2009, 95, 013704.

[39]. Krieg M, Fläschner G, Alsteens D, Gaub BM, Roos WH, Wuite GJL, Gaub HE, Gerber C, Dufrêne YF, Müller DJ, Nat. Rev. Phys 2019, 1, 41.

[40]. Zhang Y, Wei F, Poh Y-C, Jia Q, Chen J, Chen J, Luo J, Yao W, Zhou W, Huang W, Yang F, Zhang Y, Wang N, Nat. Protoc 2017, 12, 1437. [PubMed: 28686583]

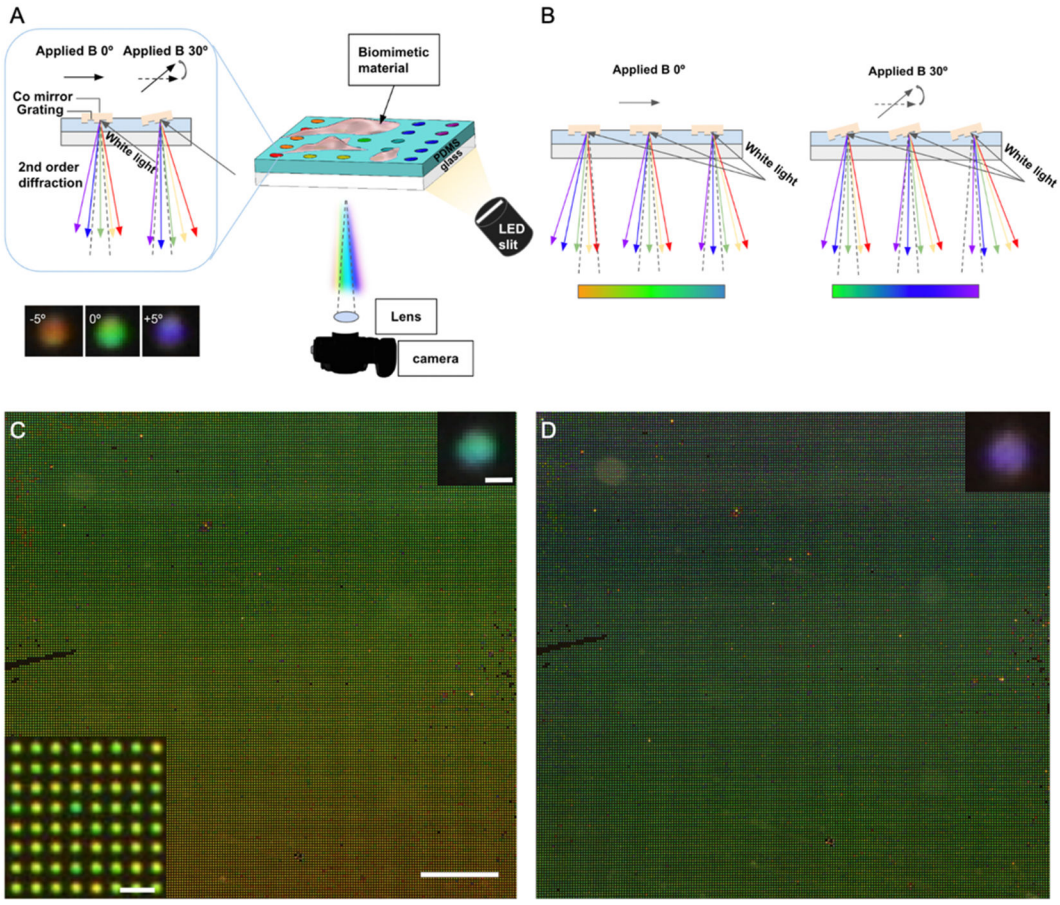

Figure 1. Illustration of the OMA platform

(A) An OMA platform consists of magnetic micromirrors with submicron optical grating structures periodically bonded on top of a soft PDMS thin film. The optical diffraction grating structure introduces color separation of the illumination light beam after reflection. A low numerical aperture (N.A.) lens is used to collect a narrow band of the reflected light rays from each micromirror for imaging (dotted lines). A zoom-in on three different micromirrors with tilting angles of −5, 0, and +5 degrees is shown in the inset (bottom left). When a uniform magnetic field is applied at a certain angle to the platform, the easy axis of the magnetic micromirrors tends to align with the external magnetic field. Each micromirror rotates differently depending on the material covering it. This rotation also results in a change in the color spectra collected for imaging. (B) The illumination color spectrum across the entire FOV before (left) and after (right) magnetic actuation. Due to the varying spatial locations of the micromirrors, the distinct illumination and diffraction angles result in different detected colors, even if each micromirror has the same tilting angle. (C) Image of an OMA platform showing a field of view of 5.1 mm × 5.5 mm before magnetic actuation and without biomimetic material attached on top. A zoomed-in area of the OMA device shows individual diffraction grating micromirrors (inset, bottom left). A further zoom on one single micromirror (inset, top right). Scale bars: (bottom right: 1 mm), (inset, bottom left: 50 μm), (inset, top right: 10 μm). (D) Image of the same OMA platform showing a clear blue shift after magnetic actuation. A further zoom-in on the single micromirror shows a

color change from Figure 1C (inset, top right). (Note: periodic artifacts may appear when using an electronic display to view these images at low resolutions. These artifacts disappear when zooming in on these images.)

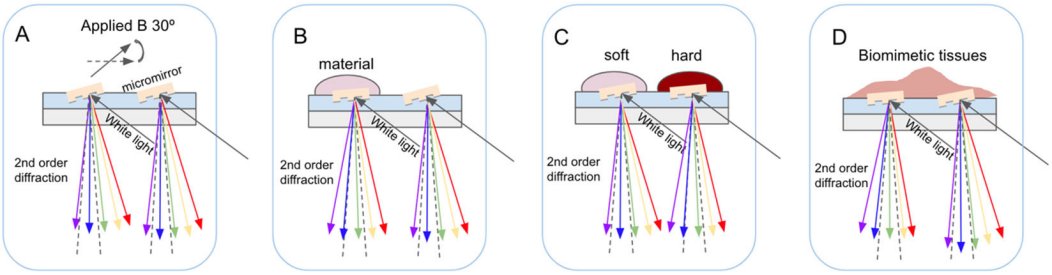

Figure 2. An illustration showing the changes in the collected color spectrum from micromirrors when measuring materials of varying stiffness and shapes.

Magnetic micromirrors on the OMA platform tilt differently depending on the materials covering them. Four different cases are illustrated as follows. In case (A), without any material on top, all micromirrors have the same tilting angle. In case (B), with material on parts of the micromirrors, those covered micromirrors have smaller tilting angles compared to those without material. In case (C), with soft and hard materials at different locations, the micromirrors with the harder material have smaller tilting angles compared to those with the softer material. In case (D), biological materials with heterogeneous stiffness on top show regions with different stiffness, resulting in varying tilting angles.

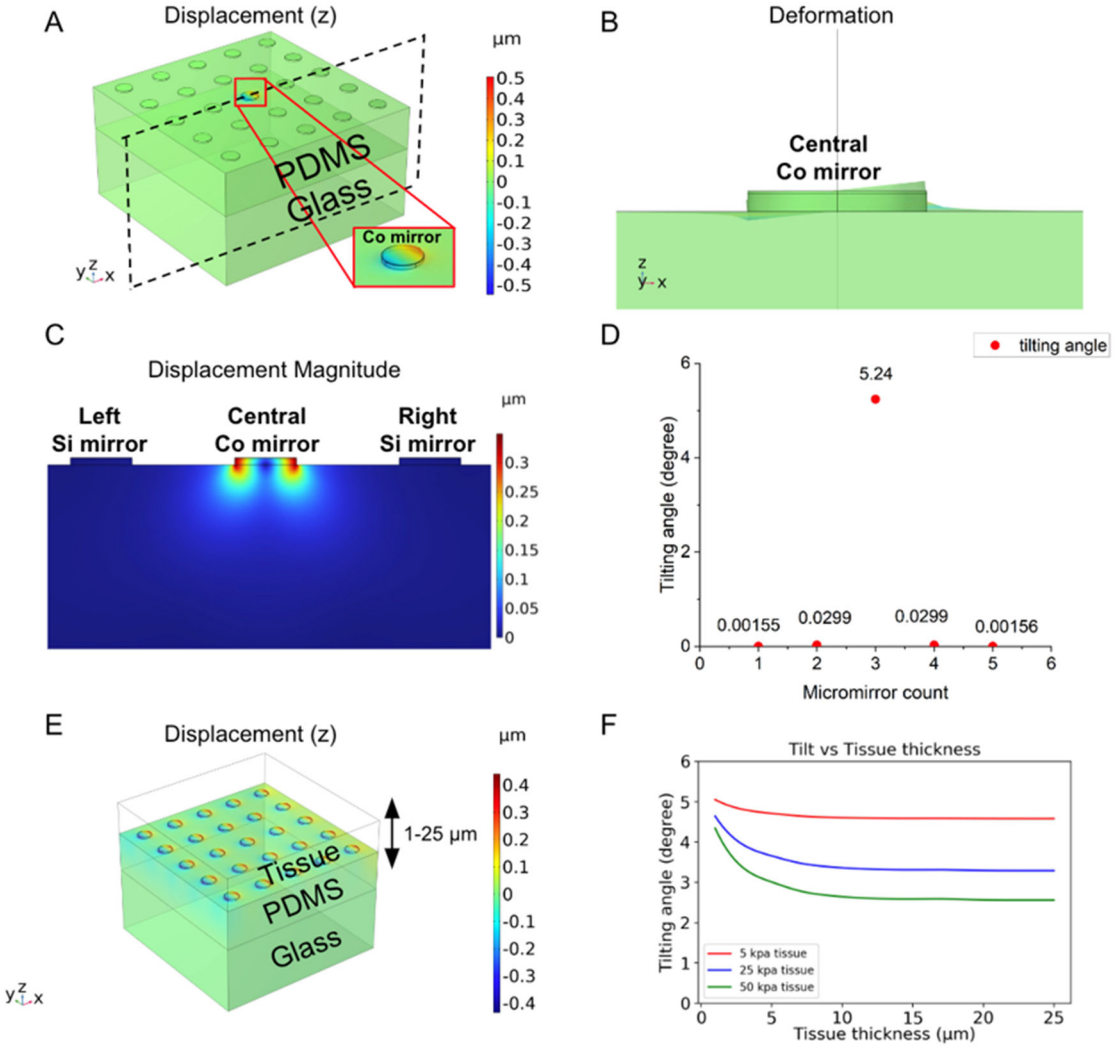

Figure 3. Simulation results of the mechanical decoupling effect between neighboring micromirrors and the effect of tissue thickness on micromirror rotation angle.

A) PDMS deformation caused by the mechanical torque applied only to the central micromirror. (B) The volumetric strain plot shows that the deformation caused by the central micromirror only affects the area within a small proximity. (C) The displacement magnitude is negligible at micromirrors adjacent to the actuated central one. (D) The tilting angle data shows that the neighboring micromirrors are affected by less than 0.1% of the central micromirror. (E) The COMSOL model illustrates 5×5 Co micromirrors sandwiched between a 5 kPa stiffness layer ranging from 1 to 25 μm in thickness and a 42 kPa PDMS substrate with a thickness of 30 μm. (F) The correlation between tissue thickness and tilting angle demonstrates that the tilting angle gradually reduces with increasing tissue thickness and reaches a plateau when the thickness exceeds 10 μm.

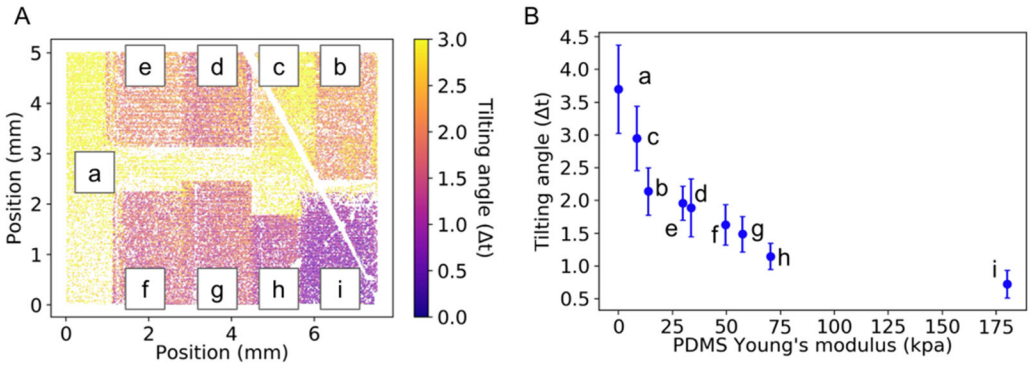

Figure 4. Stiffness measurement results.

(A) The map of tilting angle change. Each region is attached to PDMS with different stiffness and demonstrates different tilting angles. White areas depict missing or damaged micromirrors due to fabrication defects. Areas a-i represent the tilting angle change in different regions covered with PDMS of varying stiffness. (B) The correlation between tilting angle and PDMS Young's modulus.

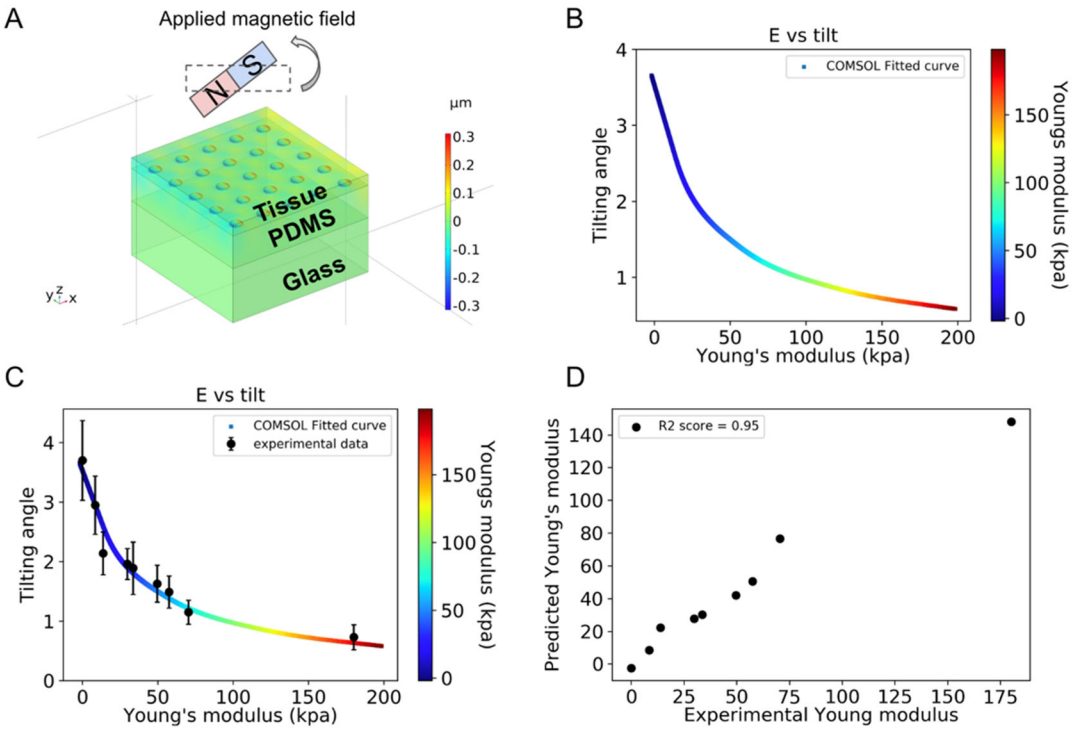

Figure 5. The correlation between micromirrors tilting angles and PDMS Young's modulus.

(A) A COMSOL model features a 5×5 Co micromirror array sandwiched between a layer of biomimetic tissue with varying Young's modulus and a PDMS substrate. The color bar indicates deformation in the z direction. (B) The correlation between the Young's modulus of biomimetic tissues and micromirrors' tilting angles, generated from the data in COMSOL and the curve fitting model (PyEarth). (C) The comparison of the simulated curve and the experimental data shows a high degree of agreement. (D) The relationship between experimentally measured (nanoindentation) PDMS Young's modulus and the simulated Young's modulus from the COMSOL-generated curve shows an R^2 score of 0.95.

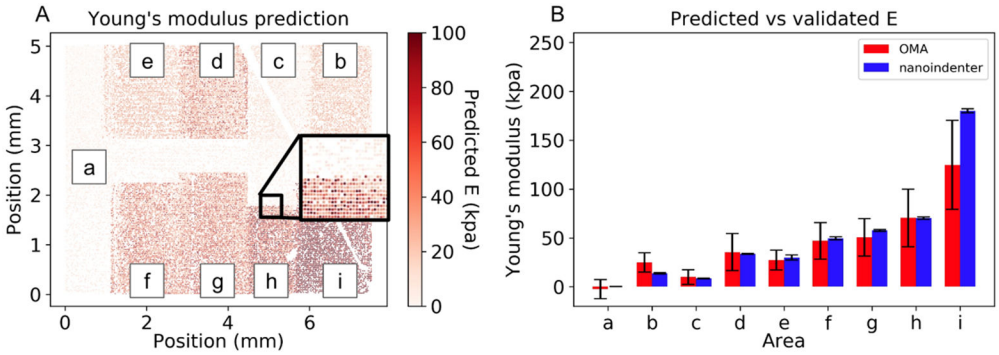

Figure 6. The PDMS stiffness distribution map.

(A) The measured stiffness distribution map on an OMA device. The clear boundaries of each area demonstrate a 26 μm resolution based on micromirror pitch, which approximates typical single mammalian cell spatial resolution. (B) The comparison between Young's modulus data measured on an OMA device and by a nanoindenter.

Table 1.

The PDMS mixing ratio and measured Young's modulus.

PDMS ratio	**No PDMS**	**Sylgard 527 A:B = 1:1**	**Sylgard 527 A:B = 5:4**	**Sylgard 527:184 = 40:1**	**Sylgard 527:184 = 30:1**	**Sylgard 527:184 = 26:1**	**Sylgard 527:184 = 20:1**	**Sylgard 527:184 = 15:1**	**Sylgard 527:184 = 10:1**	**Sylgard 527:184 = 5:1**
Measured Young's modulus (kpa)	N/A	8.48	13.74	29.80	33.59	43.15	49.54	57.45	70.31	177.99
Region in stiffness map	a	c	b	d	e	N/A	f	g	h	i